Supplementary Materials for

Global quieting of high-frequency seismic noise due to COVID-19 pandemic lockdown measures

Thomas Lecocq*, Stephen P. Hicks, Koen Van Noten, Kasper van Wijk,
Paula Koelemeijer, Raphael S. M. De Plaen, Frédérick Massin, Gregor Hillers,
Robert E. Anthony, Maria-Theresia Apoloner, Mario Arroyo-Solórzano, Jelle D. Assink,
Pinar Büyükakpınar, Andrea Cannata, Flavio Cannavo, Sebastian Carrasco,
Corentin Caudron, Esteban J. Chaves, David G. Cornwell, David Craig,
Olivier F. C. den Ouden, Jordi Diaz, Stefanie Donner, Christos P. Evangelidis,
Läslo Evers, Benoit Fauville, Gonzalo A. Fernandez, Dimitrios Giannopoulos,
Steven J. Gibbons, Társilo Girona, Bogdan Grecu, Marc Grunberg, György Hetényi,
Anna Horleston, Adolfo Inza, Jessica C. E. Irving, Mohammadreza Jamalreyhani,
Alan Kafka, Mathijs R. Koymans, Celeste R. Labedz, Eric Larose, Nathaniel J. Lindsey,
Mika McKinnon, Tobias Megies, Meghan S. Miller, William Minarik, Louis Moresi,
Víctor H. Márquez-Ramírez, Martin Möllhoff, Ian M. Nesbitt, Shankho Niyogi,
Javier Ojeda, Adrien Oth, Simon Proud, Jay Pulli, Lise Retailleau,
Annukka E. Rintamäki, Claudio Satriano, Martha K. Savage, Shahar Shani-Kadmiel,
Reinoud Sleeman, Efthimios Sokos, Klaus Stammler, Alexander E. Stott, Shiba Subedi,
Mathilde B. Sørensen, Taka'aki Taira, Mar Tapia, Fatih Turhan, Ben van der Pluijm,
Mark Vanstone, Jerome Vergne, Tommi A. T. Vuorinen, Tristram Warren,
Joachim Wassermann, Han Xiao

*Corresponding author. Email: thomas.lecocq@seismology.be

This PDF file includes:

> Materials and Methods
> Supplementary Text
> Figs. S1 to S9
> Captions for Tables S1 to S3
> Caption for Movie S1
> References

Other Supplementary Material for this manuscript includes the following:
(available at science.sciencemag.org/cgi/content/full/science.abd2438/DC1)

> Tables S1 to S3 (.xlsx)
> Movie S1 (.mp4)

Materials and Methods

Seismic ambient noise data

In this study, we consider data from vertical seismometer components. Most traditional stations comprise broadband seismometers, whilst a handful of stations comprise short-period geophones and strong-motion accelerometers (see Supplementary Files). Analysis of a subset of stations showed that using the horizontal component data of seismometers produces similar results to those from vertical components. Since most Raspberry Shake (RS) individual and school seismometer stations *(25)* comprise only single, vertical-component seismic sensors, using vertical component data in our analysis allows us to combine and compare the broadband and RS datasets. To test the applicability of citizen and school seismometer stations to study lockdown effects, we demonstrate that co-located broadband and RS sensors show similar hiFSAN drops (e.g. Figs. S8, S9). The continuous seismic data processed are available from FDSN (International Federation of Digital Seismograph Network) webservices for most stations. An overview of stations and corresponding data sources are provided in the Supplementary Text and Tables.

For many countries, especially those in China and Western Europe (e.g. UK, Belgium, Germany, Switzerland), whilst the majority of stations in the corresponding national seismic networks showed noise reductions associated with lockdown, we decided not to include every station in our global analysis to try to ensure a more uniform spatial sampling. In total, we studied data from 337 seismic stations; 185 showed clear lockdown noise-reduction indications. Stations with less obvious daytime lockdown effects, but where lockdown effects are still visible at night, are also marked as lockdown stations in the Supplementary Files. For 83 stations, we did not observe any noise level decrease associated with a lockdown or in-country emergency measures. These are labelled as blue symbols in Figure 1 in the main text and are listed separately in the Supplementary Files. For 69 stations, observation of a noise level decrease was not observed due to data gaps, station hardware problems, or by masking due to longer-term seasonal effects.

Audible sound data

In Brussels, audible sound recordings are made available by the regional environment authority "Bruxelles Environnement" (https://environnement.brussels/; last accessed July 2020). In a preprocessing step, the audible noise is convolved with the response of the human ear in the 20 Hz - 20 kHz band.

Mobility data

Mobility data are based on proprietary mobile phone usage data from Google *(41)* (https://www.google.com/covid19/mobility, last accessed July 2020) and from Apple (https://www.apple.com/covid19/mobility, last accessed July 2020). These two datasets comprise anonymized daily percentage changes for a variety of different categories, such as those based on the respective mapping apps. Google data are available from 2020-02-15; Apple data from 2020-01-13. These data are likely heavily biased by members of the population carrying their phones and actively using the mapping apps. To plot the

mobility results in figures, we combine similar mobility categories from Google and Apple:

- Transport: mean of Google's "transit stations" and Apple's "driving" and "transit"
- Retail & recreation: mean of Google's "grocery and pharmacy", "retail and recreation" and "parks"
- Workplaces: Google's "workplaces"
- Residential: Google's "residential"

The correlation coefficient r is calculated using linear least-squares regression between each mobility time series and the seismic noise data, both expressed as "percentage changes" from baseline. The baseline is defined during the pre-lockdown period for both series.

Flight data

Flight data for Barbados were retrieved for the period Nov 2019 to May 2020 from the OpenSky network archive *(42)* over a 2.8 degree longitude by 1.6 degree latitude box centered on Grantley Adams International Airport (TBPB). These flight data are freely available to researchers upon registering at the OpenSky website. The number of take-offs and landings at TBPB were computed using the methods described in Proud *(43)*. For flights that operated across midnight (UTC), the flight counted for the statistics on the day of departure for take-offs or the day of arrival for landings. Due to the method of data acquisition, some flights are not included in the dataset but this does not affect the overall pattern of flight reductions due to COVID-19. A high-level, openly available dataset of flights from January 2020 onwards over Europe, North America and, with limitations, other parts of the world is available from OpenSky (http://doi.org/10.5281/zenodo.3928550) to extend our observations and interpretations for the global data set.

Noise computation approach

The quality of seismic stations is often determined using power spectral density (PSD) estimates of their records. When aggregated over hours or days, the PSD is a reasonable quantification of the noise levels in different frequency bands. Evaluations of station noise levels at different frequencies have been carried out for decades, but this has recently been made easier for continuous time series by the release of PQLX("IRIS-PASSCAL Quick Look eXtended") *(4, 43)*.

For this study, we chose not to apply the default PQLX parameters *(44)* and apply less smoothing to obtain a finer frequency resolution together with more dynamic spectra. The PSD are computed using the ObsPy implementation *(46–48)*, equivalent to that in PQLX. A single PSD is computed from 30-minute windows with 50 percent overlap. The PSD of each windowed time series *(49)* is computed using Welch's method *(50)*. This method reduces numerical noise in the power spectra at the expense of reducing the frequency resolution because of frequency binning, but this effect is minimized with a robust smoothing parametrization. The windowed segments are then converted to a periodogram using the squared magnitude of the discrete Fourier transform. The displacement spectral power (D_{pow}) is related to the acceleration PSD in decibel (A_{dB}) by the following relation:

$$D_{pow}(f) = \frac{A_{pow}(f)}{(2\pi f)^2} = \frac{10^{\left(\frac{A_{dB}(f)}{10}\right)}}{(2\pi f)^2}$$

The RMS (root-mean-square) of the time-domain displacement (d_{rms}), bandpassed between f_{min} and f_{max}, is related to the power spectral amplitude (D_{pow}) by Parseval's identity:

$$d_{rms}(t) = \sqrt{\int_{f_{min}}^{f_{max}} D_{pow}(f) df}$$

For many stations, we tested a range of frequency bandpass filters (0.1-1.0 Hz, 1.0-20 Hz, 4-14 Hz, 4-20 Hz). Whilst the frequency spectrum of the lockdown effect might vary between different stations, we found that we were able to see the lockdown effect for most stations using the 4-14 Hz filter. The high-pass corner of the filter is set to >>1 Hz to prevent leakage of microseism, especially at island stations, many of which are included in our dataset (Figure 1). Thus, d_{rms} (t) filtered between 4 and14 Hz is the hiFSAN parameter discussed throughout the text. This frequency range allowed us to obtain a large dataset of noise changes, especially enabling 40 samples per second at higher data to be analyzed. Where only 20 samples per second seismic data were available for a handful of stations, data were bandpass filtered between 4 and 9 Hz. HE.HEL2 in Helsinki, Finland, is the only station for which d_{rms} (t) reduction was only visible between 60 and 90 Hz.

A standardized processing strategy and parameterization was defined in order to obtain global comparable results. Our processing workflow is as follows:

- selecting the seismic channel and data provider of the seismometer data of interest;
- downloading the seismic waveform data for the time period of interest;
- computing daily probabilistic PSDs (PPSD) from the downloaded data;
- processing PPSDs and extracting the RMS of the time-domain displacement of the selected time period for different frequency bands;
- manually assessingthe long-term hiFSAN;
- creating data analysis figures to demonstrate noise variation over time using different visualizations (pre-lockdown and lockdown hourly displacement variation, monthly variation). Figures were made using Matplotlib *(51)*.

Due to the heterogeneity of global seismic networks and the vast quantity of data downloading and processing required, we invited members of the seismological community via social media and traditional word-of-mouth in a democratized scientific approach *(52)*. All authors have accessed and processed seismic data following the data analysis instructions presented in the Methods Section. All authors have read and commented during the development of this manuscript. This processing workflow has been made publicly available in Jupyter Notebooks *(53)* published on GitHub *(54)*; (https://github.com/ThomasLecocq/SeismoRMS; last accessed July 2020). The final notebooks will be added to seismo-live.org *(55)*.

In this paper, we focus on computing changes in ground displacement. Similar results have been obtained by computing velocity or acceleration noise changes. For

plotting the global comparisons in Figure 2 and Figure S1, data are normalized to the 15-85th percentiles of the pre-lockdown period and clipped above the 99th percentile for remaining outliers *(40)*.

References
41. A. Aktay, et al., arXiv preprint arXiv:2004.04145(2020).
42. M. Schäfer, M. Strohmeier, V. Lenders, I. Martinovic, M.Wilhelm, IPSN-14 Proceedings of the 13th International Symposium on Information Processing in Sensor Networks (IEEE, 2014), pp. 83–94.
43. S. R. Proud, Aerospace 7, 16 (2020).
44. D. E. McNamara, R. I. Boaz, U.S. Geol. Surv. Open-File Rept 2010-1292, 41 (2010).
45. R. E. Anthony, A. T. Ringler, D. C. Wilson, M. Bahavar, K. D. Koper, Seismological Research Letters 91, 3 (2020).
46. M. Beyreuther, et al., Seismological Research Letters 81, 530 (2010).
47. T. Megies, M. Beyreuther, R. Barsch, L. Krischer, J. Wassermann, Annals of Geophysics 54, 47 (2011).
48. L. Krischer, et al., Computational Science & Discovery 8, 014003 (2015).
49. R. B. Blackman, J. W. Tukey, Bell System Technical Journal 37, 185 (1958).
50. P. Welch, IEEE Transactions on Audio and Electroacoustics 15, 70 (1967).
51. J. D. Hunter, Computing in Science & Engineering 9, 90 (2007).
52. R. Lacassin, et al., Geoscience Communication 3, 129 (2020).
53. T. Kluyver, et al., Positioning and Power in Academic Publishing: Players, Agents and Agendas, F. Loizides, B. Schmidt, eds. (IOS Press, 2016), pp. 87–90.
54. T. Lecocq, F. Massin, C. Satriano, M. Vanstone, T. Megies, SeismoRMS - A simple Python/Jupyter Notebook package for studying seismic noise changes (2020).
55. L. Krischer, et al., Seismological Research Letters 89, 2413 (2018).
56. QGIS Development Team, QGIS Geographic Information System, Open Source Geospatial Foundation (2020).

Supplementary Text

Citations for seismic networks used in this study
   This section lists the network codes (in bold) for stations analyzed in this study followed by the full citation as per the FDSN website, where available.

- **AC**: Institute of Geosciences, Energy, Water and Environment. (2002). Albanian Seismological Network [Data set]. International Federation of Digital Seismograph Networks. https://doi.org/10.7914/SN/AC
- **AF**: Penn State University. (2004). AfricaArray. International Federation of Digital Seismograph Networks. https://doi.org/10.7914/SN/AF
- **AK**: Alaska Earthquake Center, U. O. A. F. (1987). Alaska Regional Network. International Federation of Digital Seismograph Networks. https://doi.org/10.7914/SN/AK

- **AM**: (1) Raspberry Shake Community; (2) OSOP, S.A.; (3) Gempa GmbH. (2016). Raspberry Shake. (1) OSOP, S.A.; (2) gempa GmbH. https://doi.org/10.7914/SN/AM
- **AM**, Nepal: Nepal School Seismology Network, (1) http://dx.doi.org/10.5281/zenodo.3406345 and (2) Subedi S, Hetényi G, Denton P, Sauron A (2020) Seismology at School in Nepal: A program for educational and citizen seismology through a low-cost seismic network. Front Earth Sci 8:73. doi:10.3389/feart.2020.00073.
- **AU**: Geoscience Australia (GA). (1994). Australian National Seismograph Network (ANSN).
- **BE**: Royal Observatory of Belgium (1985). Belgian Seismic Network. International Federation of Digital Seismograph Networks. https://doi.org/10.7914/SN/BE
- **BK**: Northern California Earthquake Data Center. (2014). Berkeley Digital Seismic Network (BDSN) [Data set]. Northern California Earthquake Data Center. https://doi.org/10.7932/BDSN
- **BL**: Universidade de Sao Paulo, USP. (1988). Brazilian Lithospheric Seismic Project (BLSP).
- **BW**: Department of Earth and Environmental Sciences, Geophysical Observatory, Ludwig-Maximilians-Universität München (2001), BayernNetz. International Federation of Digital Seismograph Networks. https://doi.org/10.7914/SN/BW.
- **BX**: Department of Geological Survey of Botswana. (2001). Botswana Seismological Network (BSN).
- **C1**: Universidad de Chile. (2013). Red Sismologica Nacional. International Federation of Digital Seismograph Networks. https://doi.org/10.7914/SN/C1
- **CA**: Institut Cartogràfic I Geològic De Catalunya, Institut d'Estudis Catalans (1984). Catalan Seismic Network [Data set]. International Federation of Digital Seismograph Networks. https://doi.org/10.7914/SN/CA
- **CH**: Swiss Seismological Service (SED) At ETH Zurich. (1983). National Seismic Networks of Switzerland. ETH Zürich. https://doi.org/10.12686/sed/networks/ch
- **CI**: California Institute of Technology and U.S. Geological Survey (USGS) Pasadena. (1926). Southern California Seismic Network. International Federation of Digital Seismograph Networks. https://doi.org/10.7914/SN/CI
- **CN**: Geological Survey of Canada. (1989). Canadian National Seismograph Network. International Federation of Digital Seismograph Networks. https://doi.org/10.7914/SN/CN
- **CQ**: Geological Survey Department Cyprus. (2013). Cyprus Broadband Seismological Network. International Federation of Digital Seismograph Networks. https://doi.org/10.7914/SN/CQ
- **CU**: Albuquerque Seismological Laboratory (ASL)/ U.S. Geological Survey (USGS). (2006). Caribbean USGS Network. International Federation of Digital Seismograph Networks. https://doi.org/10.7914/SN/CU
- **EI**: INSN. (1993). Irish National Seismic Network, operated by the Dublin Institute for Advanced Studies and supported by the Geological Survey Ireland.

International Federation of Digital Seismograph Networks.
https://doi.org/10.7914/SN/EI

- **FR**: RESIF. (1995). RESIF-RLBP French Broad-band network, RESIF-RAP strong motion network and other seismic stations in metropolitan France [Data set]. RESIF - Réseau Sismologique et géodésique Français. https://doi.org/10.15778/RESIF.FR
- **G**: Institut de Physique du Globe de Paris (IPGP), & Ecole et Observatoire des Sciences de La Terre de Strasbourg (EOST). (1982). GEOSCOPE, French Global Network of broadband seismic stations. Institut de Physique du Globe de Paris (IPGP). https://doi.org/10.18715/GEOSCOPE.G
- **GB**: British Geological Survey. (1970). Great Britain Seismograph Network. Contains British Geological Survey materials © UKRI [2020].
- **GE**: GEOFON Data Centre. (1993). GEOFON Seismic Network. Deutsches GeoForschungsZentrum GFZ. https://doi.org/10.14470/TR560404
- **GO**: Ilia State University- Seismic Monitoring Centre of Georgia (Georgia). (1988). National Seismic Network of Georgia.
- **GR**: Federal Institute for Geosciences and Natural Resources (BGR). (1976). German Regional Seismic Network (GRSN). Federal Institute for Geosciences and Natural Resources (BGR). https://doi.org/10.25928/mbx6-hr74
- **GT**: Albuquerque Seismological Laboratory (ASL)/USGS. (1993). Global Telemetered Seismograph Network (USAF/USGS). International Federation of Digital Seismograph Networks. https://doi.org/10.7914/SN/GT
- **HE**: Institute of Seismology, U. O. H. (1980). The Finnish National Seismic Network. GFZ Data Services. https://doi.org/10.14470/UR044600
- **HL**: National Observatory of Athens, I. O. G. (1997). National Observatory of Athens Seismic Network. International Federation of Digital Seismograph Networks. https://doi.org/10.7914/SN/HL
- **HT**: Aristotle University of Thessaloniki Seismological Network. (1981). Permanent Regional Seismological Network operated by the Aristotle University of Thessaloniki. International Federation of Digital Seismograph Networks. https://doi.org/10.7914/SN/HT
- **IC**: Albuquerque Seismological Laboratory (ASL)/USGS. (1992). New China Digital Seismograph Network. International Federation of Digital Seismograph Networks. https://doi.org/10.7914/SN/IC
- **II**: Scripps Institution of Oceanography. (1986). IRIS/IDA Seismic Network. International Federation of Digital Seismograph Networks. https://doi.org/10.7914/SN/II
- **IM**: (1965). International Miscellaneous Stations (IMS).
- **IN**: India Meteorological Department. (2000). National Seismic Network of India.
- **IU**: Albuquerque Seismological Laboratory (ASL)/USGS. (1988). Global Seismograph Network (GSN - IRIS/USGS). International Federation of Digital Seismograph Networks. https://doi.org/10.7914/SN/IU
- **IV**: INGV Seismological Data Centre. (2006). Rete Sismica Nazionale (RSN). Istituto Nazionale di Geofisica e Vulcanologia (INGV), Italy. https://doi.org/10.13127/SD/X0FXnH7QfY

- **KO**: Bogazici University Kandilli Observatory and Earthquake Research Institute. (2001). Bogazici University Kandilli Observatory and Earthquake Research Institute. International Federation of Digital Seismograph Networks. https://doi.org/10.7914/SN/KO
- **KV**: Oth, A., Barrière, J., D'Oreye, N., Mavonga, G., Subira, J., Mashagiro, N., Kafundu, B., Fiama, S., Celli, G., De Dieu Birigande, J., Ntenge, A. J., & Kervyn, F. (2013). Kivu Seismological Network (KivuSnet). Deutsches GeoForschungsZentrum GFZ. https://doi.org/10.14470/XI058335
- **LD**: Lamont Doherty Earth Observatory (LDEO), Columbia University. (1970). Lamont-Doherty Cooperative Seismographic Network (LCSN). https://doi.org/10.7914/SN/LD
- **MD**: Geological and Seismological Institute of Moldova. (2007). Moldova Digital Seismic Network. International Federation of Digital Seismograph Networks. https://doi.org/10.7914/SN/MD
- **MN**: MedNet Project Partner Institutions. (1990). Mediterranean Very Broadband Seismographic Network (MedNet). Istituto Nazionale di Geofisica e Vulcanologia (INGV). https://doi.org/10.13127/SD/fBBBtDtd6q
- **MQ**: Institut de Physique du Globe de Paris. (1935) The data used in this study were acquired by the Volcanological and Seismological of Martinique (OVSM) via the VOLOBSIS Portal : http://volobsis.ipgp.fr.
- **MX**: SSN (2017). Servicio Sismológico Nacional, Instituto de Geofísica, Universidad Nacional Autónoma de México, México. https://doi.org/10.21766/SSNMX/SN/MX
- **NC**: USGS Menlo Park. (1967). USGS Northern California Network. International Federation of Digital Seismograph Networks. https://doi.org/10.7914/SN/NC
- **NE**: Albuquerque Seismological Laboratory (ASL)/USGS. (1994). New England Seismic Network. International Federation of Digital Seismograph Networks. https://doi.org/10.7914/SN/NE
- **NL**: KNMI. (1993). Netherlands Seismic and Acoustic Network. Royal Netherlands Meteorological Institute (KNMI). https://doi.org/10.21944/e970fd34-23b9-3411-b366-e4f72877d2c5
- **NP**: USGS Earthquake Science Center. (1931). U.S. National Strong-Motion Network. International Federation of Digital Seismograph Networks. https://doi.org/10.7914/SN/NP
- **NS**: University of Bergen (1982), Norwegian National Seismic Network.
- **NZ**: Institute of Geological & Nuclear Sciences Ltd (GNS New Zealand). (1988). New Zealand National Seismograph Network. We acknowledge the New Zealand GeoNet project and its sponsors EQC, GNS Science and LINZ, for providing data/images used in this study.
- **OE**: ZAMG-Zentralanstalt Für Meterologie Und Geodynamik. (1987). Austrian Seismic Network. International Federation of Digital Seismograph Networks. https://doi.org/10.7914/SN/OE
- **PA**: Red Sismica Volcan Baru. (2000). ChiriNet [Data set]. International Federation of Digital Seismograph Networks. https://doi.org/10.7914/SN/PA

- **PF**: Institut de Physique du Globe de Paris (1980). Piton de la Fournaise Volcano Observatory Network (Reunion Island) (OVPF). The data used in this study were acquired by the Volcanological and Seismological of Observatory of Piton de la Fournaise (OVPF) via the VOLOBSIS Portal : http://volobsis.ipgp.fr.
- **PT**: Pacific Tsunami Warning Center (1965). Pacific Tsunami Warning Seismic System
- **QM**: Bureau de Recherches Géologiques et Minières (BRGM). (2019). Comoros Seismic Network (Comoros Seismic Network). The Mayotte station KNKL (QM) was installed through Tellus Mayotte project (CNRS-INSU) and their data were made available to LR through REVOSIMA.
- **OV**: Protti, M. (1984). Observatorio Vulcanológico y Sismológico de Costa Rica [Data set]. International Federation of Digital Seismograph Networks. https://doi.org/10.7914/SN/OV.
- **RO**: National Institute for Earth Physics (NIEP Romania). (1994). Romanian Seismic Network. International Federation of Digital Seismograph Networks. https://doi.org/10.7914/SN/RO
- **S1**: Australian National University (ANU, Australia). (2011). Australian Seismometers in Schools [Data set]. Australian Passive Seismic Server - Australian National University. https://doi.org/10.7914/SN/S1.
- **SV**: Servicio Nacional de Estudios Territoriales (SNET El Salvador). (2004). Servicio Nacional de Estudios Territoriales (SNET), El Salvador (SNET-BB)
- **TC**: (2016). Universidad de Costa Rica. https://doi.org/10.15517/TC
- **US**: Albuquerque Seismological Laboratory (ASL)/USGS. (1990). U.S. National Seismic Network. International Federation of Digital Seismograph Networks. https://doi.org/10.7914/SN/US
- **YS**: Diaz, J., and Schimmel, M. (2019). SANIMS [Data set]. International Federation of Digital Seismograph Networks. https://doi.org/10.7914/SN/YS_2019
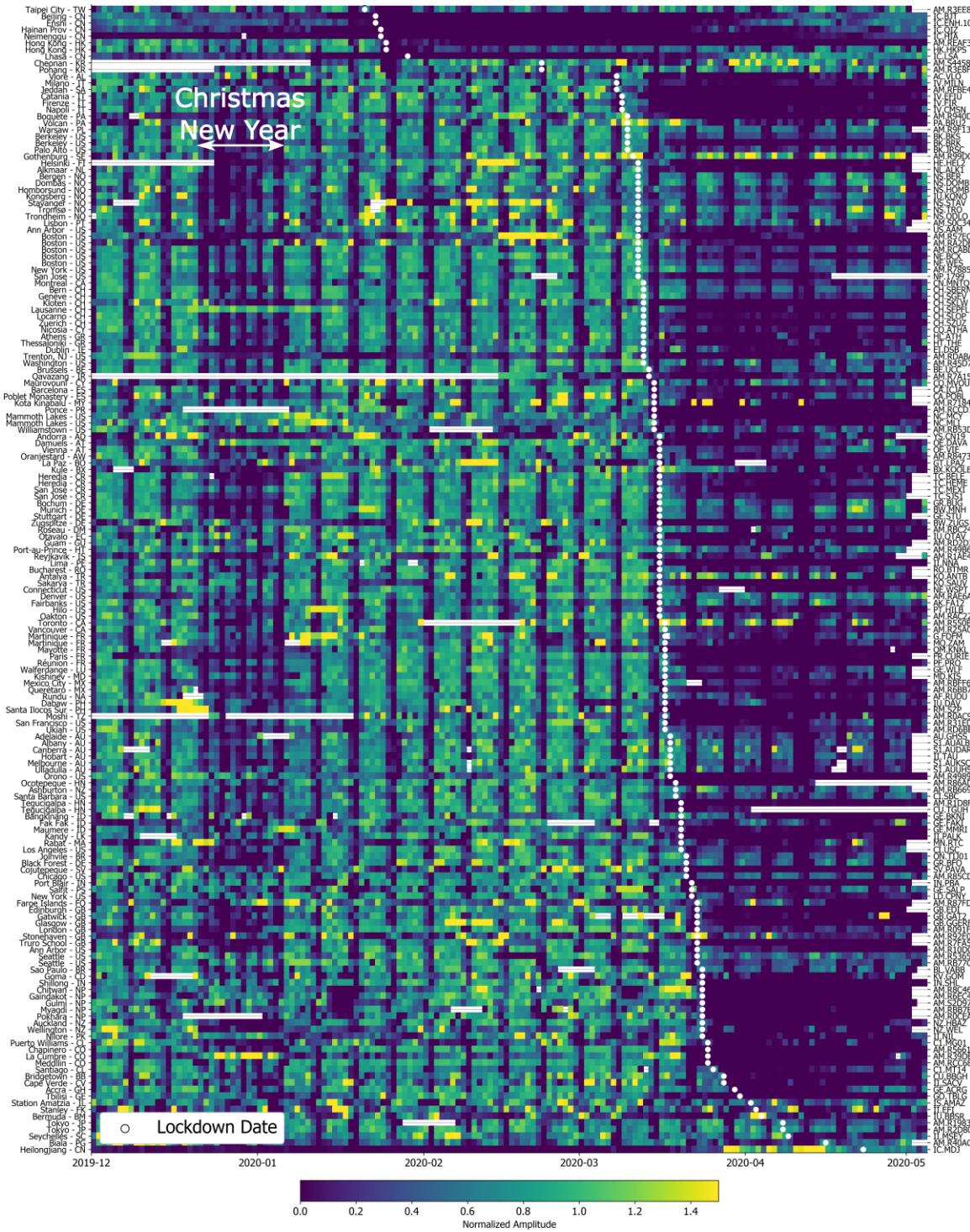
Fig. S1. Global temporal changes in seismic noise.

Global daily median hiFSAN based on displacement data, normalized to percentage variation of the baseline before lockdown measures, and sorted by lockdown date. Data gaps are colored white. Location and country code of the station are indicated on the left; network and station codes on the right. Stations with long data gaps over the period are not shown.
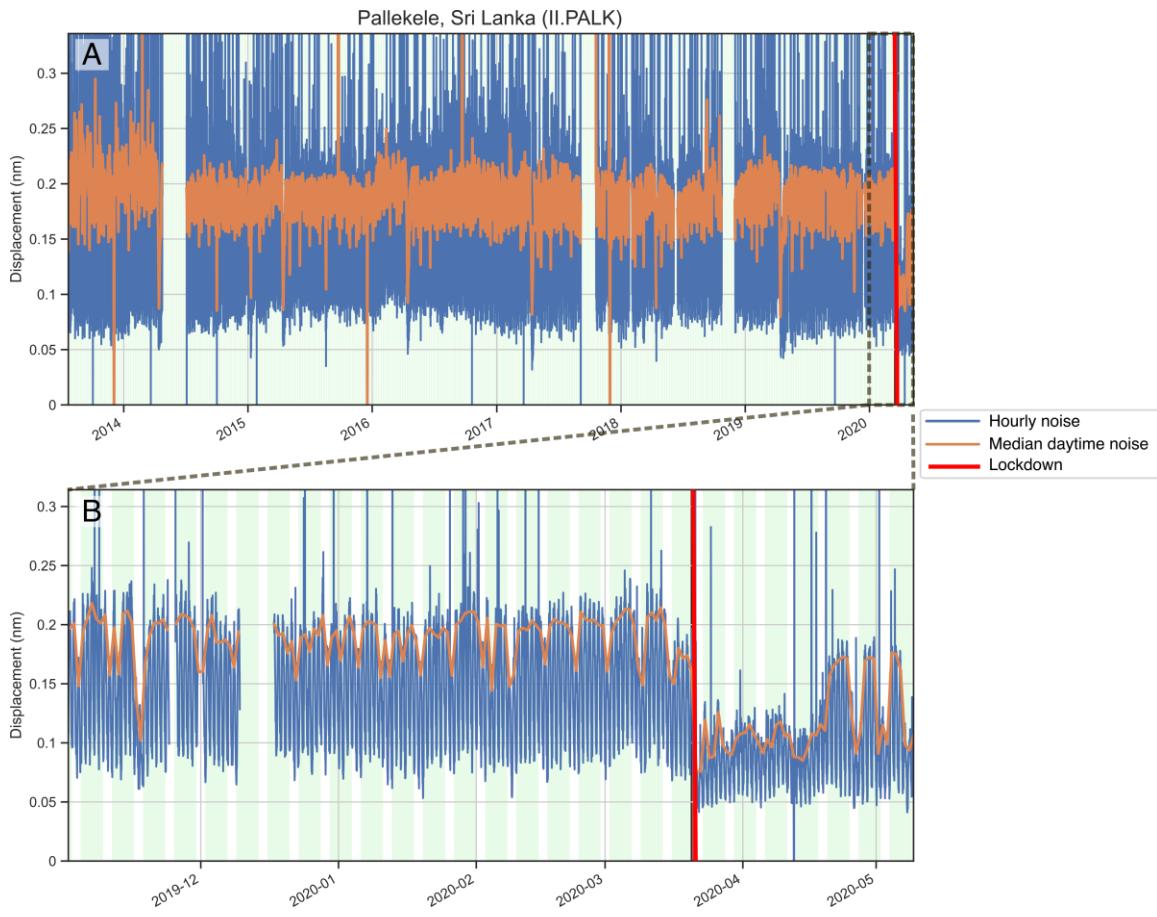
Fig. S2. Long-term evolution of hiFSAN in Sri Lanka.
A) Long-term seismic noise evolution. B) Zoom-in of noise in 2020.
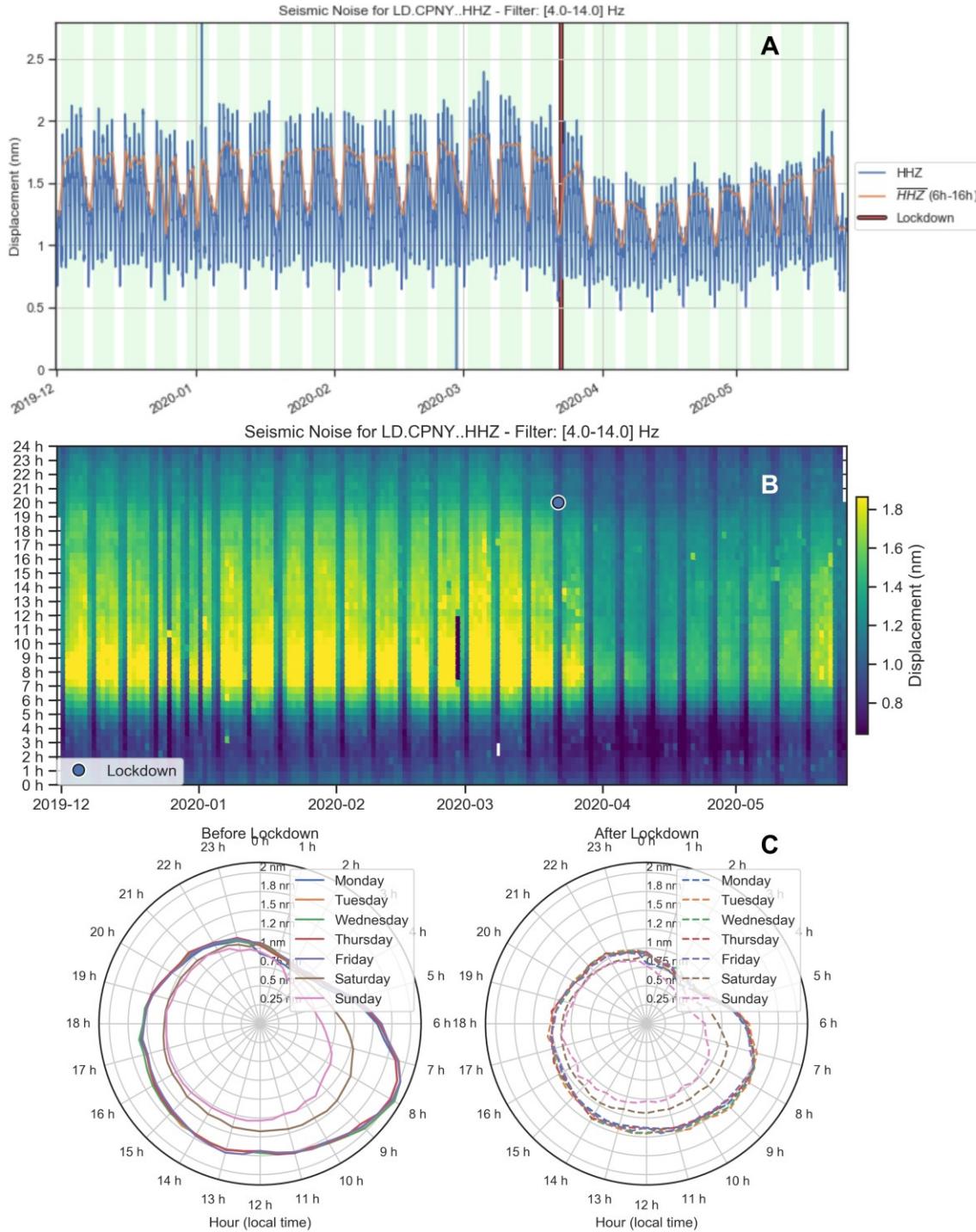
Fig. S3. Lockdown effects on seismic noise in Central Park, NY.

(A) Evolution of seismic noise at station LD.CPNY in Central Park, New York for the Dec 2019 - May 2020 period based on displacement data. (B) The same as (A) but shown in an hourly grid representation. (C) 24h clock plots showing average displacement variation for each day of the week for the period before lockdown (left) and after lockdown started (right).
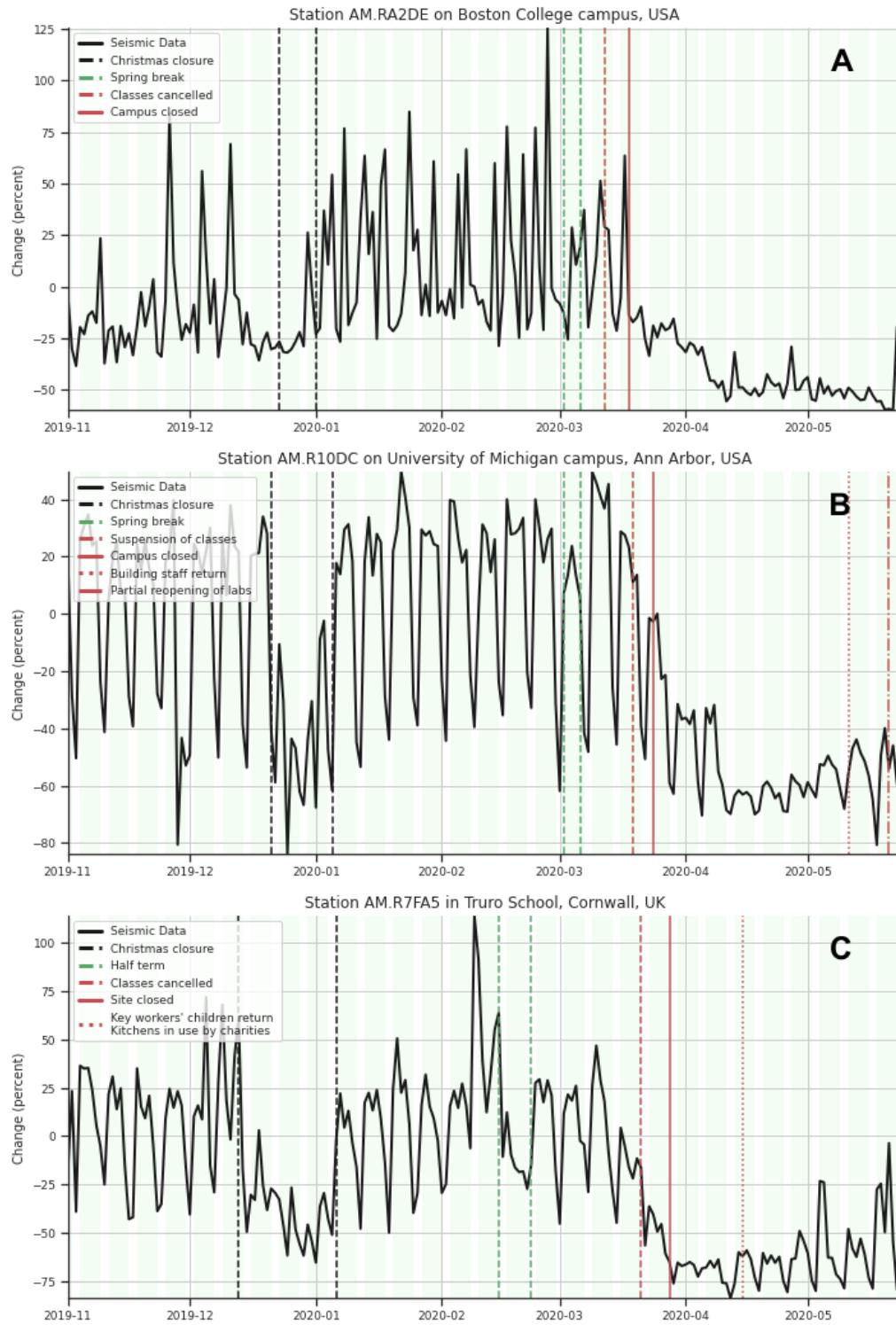
Fig. S4. Temporal changes in hiFSAN at schools and universities.
(A) Boston College (US). (B) University of Michigan campus (US). (C) Truro School
(Cornwall, UK). Time periods like the Christmas break and Spring break / half term are
easily identified as periods of lower seismic noise. Note the large drop in hiFSAN up to
more than 50 % change after classes are cancelled and campuses are closed.
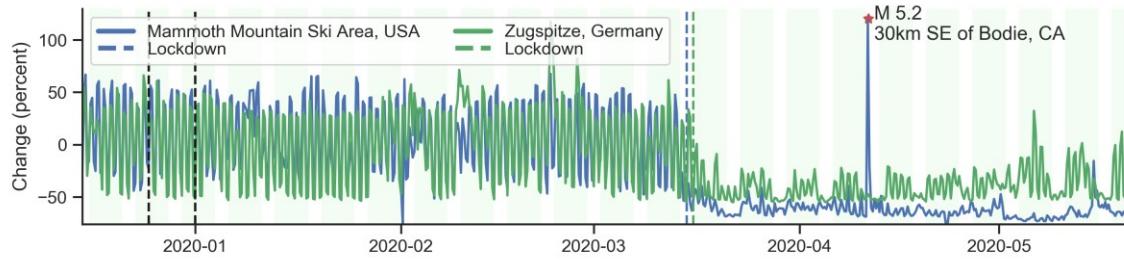
Fig. S5. Lockdown effects on seismic noise in touristic ski resort areas.

Temporal changes of hiFSAN at two touristic ski resort areas: Mammoth Mountain (USA - station NC.MCY) and Zugspitze (Germany, station BW.ZUGS), showing the effect of the complete stop of the resorts' lifts or cog-wheel railway
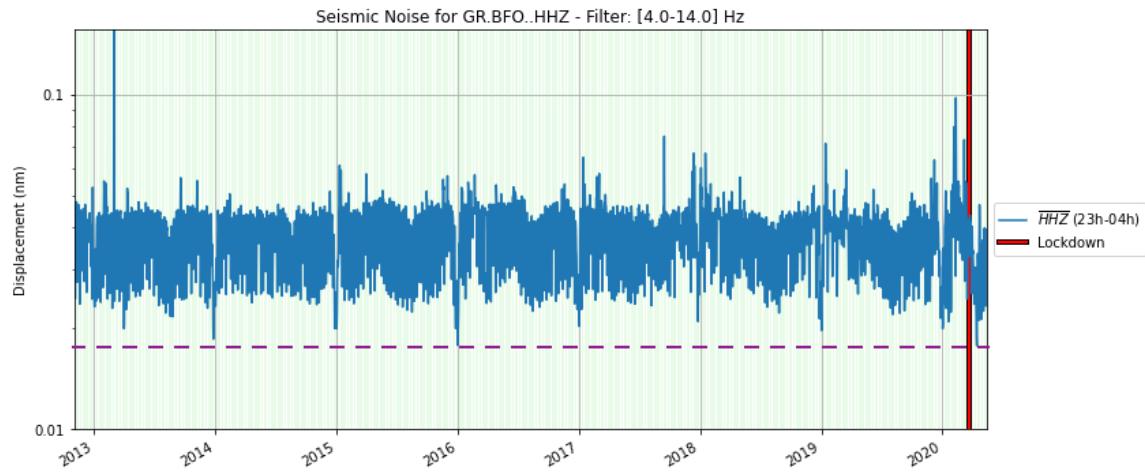
Fig. S6. Temporal changes in hiFSAN at the Black Forest Observatory, Germany.
Long-term noise evolution at the Black Forest Observatory, Germany (GR.BFO) based
on median nighttime (23:00-04:00) RMS noise from displacement data. The purple
dashed line indicates the minimum noise observed during the 2020 lockdown period.
Note the logarithmic y-axis.
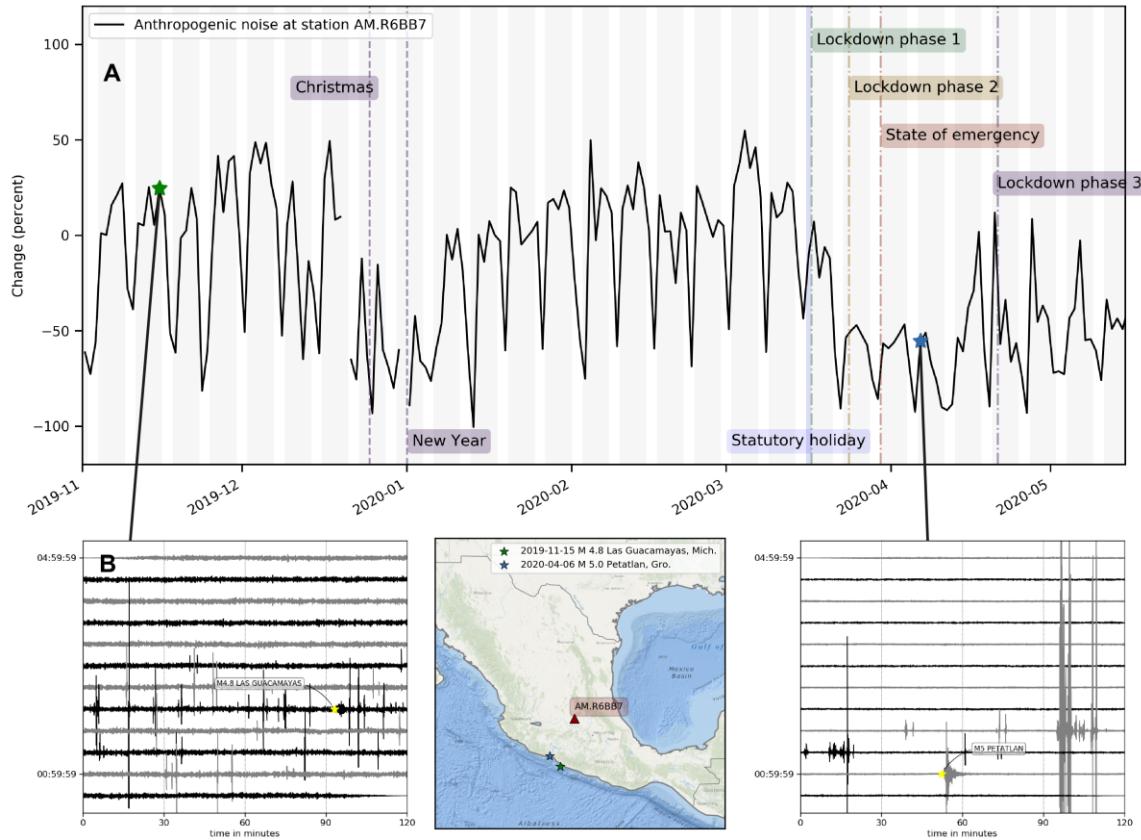
Fig. S7. Increased earthquake detection capability in Mexico.

(A) Temporal changes in hiFSAN at Raspberry Shake station AM.R6BB7 (city center of Querétaro, Mexico). (B) Earthquakes at Las Guacamayas (15/11/2019, M4.8 and 28 km depth) and Petatlan (07/04/2020, M5.0 and 15 km depth) recorded before (left column) and after the lockdown (right). The insert in the center indicates the locations of the earthquakes and Raspberry Shake station.

16
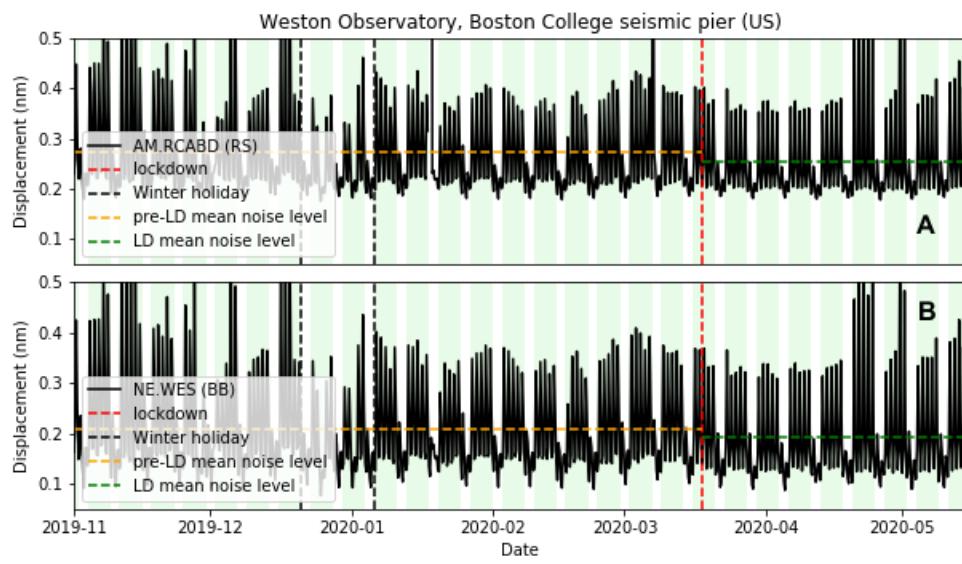
Fig. S8. Comparison of lockdown effects on Raspberry Shake and broadband stations on the surface.

Temporal changes in seismic noise at the co-located AM.RCABD Raspberry Shake station (A) and NE.WES broadband station (B) at the Weston Observatory, Boston College seismic pier in the United States of America.
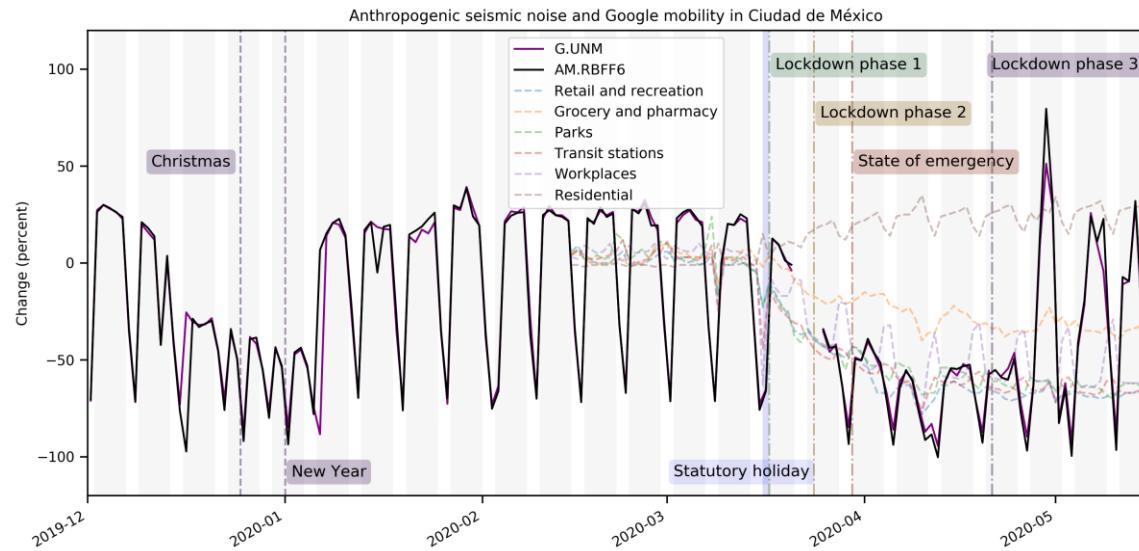
Fig. S9. Comparison of lockdown effects on Raspberry Shake and broadband stations in a borehole.

Temporal changes in hiFSAN at broadband station G.UNM and Raspberry Shake station AM.RBFF6, both installed in a 20m deep borehole in the Ciudad Universitaria in Mexico City. Google mobility data for the city are shown for comparison as dashed lines.

Movie S1

Movie version of Figure 2 and Figure S1. The time evolution of the amplitude of hiFSAN for each station is shown as bars with variable height. The lockdown dates (LD1) for each country appear on the left side.

Introduction to the Tables

The supplementary tables give an overview of the seismic stations for which data were analyzed in this study. Each author provided lockdown (LD) information (DateLD1, TimeLD1, DateLD2, TimeLD2) for the seismometer location. Population density data show interpolated estimates of human population count for the year 2020 *(30)*. These grid data are consistent with national census and population registers. *popden30s* gives population counts within 30 arc-second grid cells (cell size of roughly 1 km at the equator); *popden2.5min* gives population counts within 2.5 arc-minute grid cells (cell size of roughly 5 km at the equator; the inverse of this data column is used in Fig. 1). Population data for each station were extracted from grid data using QGIS *(56)*. Station locations (latitude, longitude) in all tables were extracted from FDSN websites. The three files contain:

Additional Data table S1 (separate file)

Stations where lockdown noise reduction was observed; these 185 stations are shown in Figures 1 and 4 and in Figure S1; 'yes' in *columnplottedinfig2* indicates that the station was displayed in Figure 2; 'No/double' means that another close by station in the area of interest is used;

Additional Data table S2 (separate file)

Stations where lockdown noise reduction was not observed. These 83 stations are also shown in Figure 1;

Additional Data table S3 (separate file)

Stations where data gaps, station hardware problems, or longer-term seasonal effects prohibited a conclusion on noise changes. These 69 stations are not plotted in Figure 1.

References and Notes

1. J. N. Brune, J. Oliver, The seismic noise of the earth's surface. *Bull. Seismol. Soc. Am.* **49**, 349–353 (1959).

2. R. K. Cessaro, Sources of primary and secondary microseisms. *Bull. Seismol. Soc. Am.* **84**, 142–148 (1994).

3. N. M. Shapiro, M. Campillo, Emergence of broadband Rayleigh waves from correlations of the ambient seismic noise. *Geophys. Res. Lett.* **31**, L07614 (2004). doi:10.1029/2004GL019491

4. D. E. McNamara, R. P. Buland, Ambient Noise Levels in the Continental United States. *Bull. Seismol. Soc. Am.* **94**, 1517–1527 (2004). doi:10.1785/012003001

5. J. C. Groos, J. R. Ritter, Time domain classification and quantification of seismic noise in an urban environment. *Geophys. J. Int.* **179**, 1213–1231 (2009). doi:10.1111/j.1365-246X.2009.04343.x

6. C. M. Boese, L. Wotherspoon, M. Alvarez, P. Malin, Analysis of Anthropogenic and Natural Noise from Multilevel Borehole Seismometers in an Urban Environment, Auckland, New Zealand. *Bull. Seismol. Soc. Am.* **105**, 285–299 (2015). doi:10.1785/0120130288

7. D. N. Green, I. D. Bastow, B. Dashwood, S. E. Nippress, Characterizing Broadband Seismic Noise in Central London. *Seismol. Res. Lett.* **88**, 113–124 (2017). doi:10.1785/0220160128

8. C. L. Ashenden, J. M. Lindsay, S. Sherburn, I. E. M. Smith, C. A. Miller, P. E. Malin, Some challenges of monitoring a potentially active volcanic field in a large urban area: Auckland volcanic field, New Zealand. *Nat. Hazards* **59**, 507–528 (2011). doi:10.1007/s11069-011-9773-0

9. N. Riahi, P. Gerstoft, The seismic traffic footprint: Tracking trains, aircraft, and cars seismically. *Geophys. Res. Lett.* **42**, 2674–2681 (2015). doi:10.1002/2015GL063558

10. N. J. Lindsey, S. Yuan, A. Lellouch, L. Gualtieri, T. Lecocq, B. Biondi, City-scale dark fiber DAS measurements of infrastructure use during the COVID-19 pandemic. *Geophys. Res. Lett.* **47**, e2020GL089931 (2020). doi:10.1029/2020GL089931 Medline

11. J. Díaz, M. Ruiz, P. S. Sánchez-Pastor, P. Romero, Urban seismology: On the origin of earth vibrations within a city. *Sci. Rep.* **7**, 15296 (2017). doi:10.1038/s41598-017-15499-y Medline

12. P. Denton, S. Fishwick, V. Lane, D. Daly, Football Quakes as a Tool for Student Engagement. *Seismol. Res. Lett.* **89**, 1902–1907 (2018). doi:10.1785/0220180078

13. D. Wilson *et al.*, Broadband Seismic Background Noise at Temporary Seismic Stations Observed on a Regional Scale in the Southwestern United States. *Bull. Seismol. Soc. Am.* **92**, 3335–3342 (2002). doi:10.1785/0120010234

14. C. Sohrabi *et al.*, World Health Organization declares global emergency: A review of the 2019 novel coronavirus (COVID-19). *Int. J. Surg.* **76**, 71–76 (2020). doi:10.1016/j.ijsu.2020.02.034

15. R. M. Anderson, H. Heesterbeek, D. Klinkenberg, T. D. Hollingsworth, How will country-based mitigation measures influence the course of the COVID-19 epidemic? *Lancet* **395**, 931–934 (2020). [doi:10.1016/S0140-6736(20)30567-5](doi:10.1016/S0140-6736(20)30567-5) Medline

16. M. Nicola *et al*., Evidence based management guideline for the COVID-19 pandemic. *Int. J. Surg.* **77**, 206–216 (2020). doi:10.1016/j.ijsu.2020.04.001

17. T. Laing, The economic impact of the Coronavirus 2019 (Covid-2019): Implications for the mining industry. *Extr. Ind. Soc.* **7**, 580–582 (2020). doi:10.1016/j.exis.2020.04.003

18. A. Hoque, F. A. Shikha, M. W. Hasanat, I. Arif, A. B. A. Hamid, The Effect of Coronavirus (COVID-19) in the Tourism Industry in China. *Asian J. Multidiscip. Stud.* **3**, 52–58 (2020).

19. M. U. G. Kraemer, C.-H. Yang, B. Gutierrez, C.-H. Wu, B. Klein, D. M. Pigott, L. du Plessis, N. R. Faria, R. Li, W. P. Hanage, J. S. Brownstein, M. Layan, A. Vespignani, H. Tian, C. Dye, O. G. Pybus, S. V. Scarpino; Open COVID-19 Data Working Group, The effect of human mobility and control measures on the COVID-19 epidemic in China. *Science* **368**, 493–497 (2020). doi:10.1126/science.abb4218 Medline

20. H. Tian, Y. Liu, Y. Li, C.-H. Wu, B. Chen, M. U. G. Kraemer, B. Li, J. Cai, B. Xu, Q. Yang, B. Wang, P. Yang, Y. Cui, Y. Song, P. Zheng, Q. Wang, O. N. Bjornstad, R. Yang, B. T. Grenfell, O. G. Pybus, C. Dye, An investigation of transmission control measures during the first 50 days of the COVID-19 epidemic in China. *Science* **368**, 638–642 (2020). doi:10.1126/science.abb6105 Medline

21. J. Zhang, M. Litvinova, Y. Liang, Y. Wang, W. Wang, S. Zhao, Q. Wu, S. Merler, C. Viboud, A. Vespignani, M. Ajelli, H. Yu, Changes in contact patterns shape the dynamics of the COVID-19 outbreak in China. *Science* **368**, 1481–1486 (2020). doi:10.1126/science.abb8001 Medline

22. M. Chinazzi, J. T. Davis, M. Ajelli, C. Gioannini, M. Litvinova, S. Merler, A. Pastore Y Piontti, K. Mu, L. Rossi, K. Sun, C. Viboud, X. Xiong, H. Yu, M. E. Halloran, I. M. Longini Jr., A. Vespignani, The effect of travel restrictions on the spread of the 2019 novel coronavirus (COVID-19) outbreak. *Science* **368**, 395–400 (2020). Medline

23. M. Bauwens, S. Compernolle, T. Stavrakou, J.-F. Müller, J. Gent, H. Eskes, P. F. Levelt, R. A, J. P. Veefkind, J. Vlietinck, H. Yu, C. Zehner, Impact of Coronavirus Outbreak on NO_2 Pollution Assessed Using TROPOMI and OMI Observations. *Geophys. Res. Lett.* **47**, 11 (2020). [doi:10.1029/2020GL087978](doi:10.1029/2020GL087978)

24. Materials and methods and network citations are available as supplementary materials.

25. R. E. Anthony, A. T. Ringler, D. C. Wilson, E. Wolin, Do Low-Cost Seismographs Perform Well Enough for Your Network? An Overview of Laboratory Tests and Field Observations of the OSOP Raspberry Shake 4D. *Seismol. Res. Lett.* **90**, 219–228 (2019). [doi:10.1785/0220180251](doi:10.1785/0220180251)

26. H. Xiao, Z. C. Eilon, C. Ji, T. Tanimoto, COVID-19 Societal Response Captured by Seismic Noise in China and Italy. *Sesimol. Res. Lett.* 10.1785/0220200147 (2020). https://doi.org/10.1785/0220200147

27. P. Poli, J. Boaga, I. Molinari, V. Cascone, L. Boschi, The 2020 coronavirus lockdown and seismic monitoring of anthropic activities in Northern Italy. *Sci. Rep.* **10**, 9404 (2020). doi:10.1038/s41598-020-66368-0 Medline

28. H. Lau, V. Khosrawipour, P. Kocbach, A. Mikolajczyk, J. Schubert, J. Bania, T. Khosrawipour, The positive impact of lockdown in Wuhan on containing the COVID-19 outbreak in China. *J. Travel Med.* **27**, taaa037 (2020). doi:10.1093/jtm/taaa037

29. S. Sherburn, B. J. Scott, J. Olsen, C. Miller, Monitoring seismic precursors to an eruption from the Auckland Volcanic Field, New Zealand. *N. Z. J. Geol. Geophys.* **50**, 1–11 (2007). doi:10.1080/00288300709509814

30. Center for International Earth Science Information Network CIESIN Columbia University, Gridded population of the world, version 4 (GPWv4): Population density. Revision 11, accessed 2 June 2020 (2018); https://doi.org/10.7927/H49C6VHW.

31. W. Zürn, J. Exß, H. Steffen, C. Kroner, T. Jahr, M. Westerhaus, On reduction of long-period horizontal seismic noise using local barometric pressure. *Geophys. J. Int.* **171**, 780–796 (2007). doi:10.1111/j.1365-246X.2007.03553.x

32. B. Gutenberg, C. F. Richter, Frequency of earthquakes in California. *Bull. Seismol. Soc. Am.* **34**, 185–188 (1944).

33. Z. E. Ross, D. T. Trugman, E. Hauksson, P. M. Shearer, Searching for hidden earthquakes in Southern California. *Science* **364**, 767–771 (2019). doi:10.1126/science.aaw6888 Medline

34. E. S. Cochran, To catch a quake. *Nat. Commun.* **9**, 2508 (2018). doi:10.1038/s41467-018-04790-9 Medline

35. G. J. H. McCall, Geohazards and the urban environment. *Geol. Soc. London Eng. Geol. Spec. Publ.* **15**, 309–318 (1998). doi:10.1144/GSL.ENG.1998.015.01.31

36. M. Lehujeur, J. Vergne, J. Schmittbuhl, A. Maggi, Characterization of ambient seismic noise near a deep geothermal reservoir and implications for interferometric methods: A case study in northern Alsace, France. *Geotherm. Energy* **3**, 3 (2015). doi:10.1186/s40517-014-0020-2

37. G. Hillers, M. Campillo, Y.-Y. Lin, K.-F. Ma, P. Roux, Anatomy of the high-frequency ambient seismic wave field at the TCDP borehole. *J. Geophys. Res.* **117**, B06301 (2012). doi:10.1029/2011JB008999

38. M. Picozzi, S. Parolai, D. Bindi, A. Strollo, Characterization of shallow geology by high-frequency seismic noise tomography. *Geophys. J. Int.* **176**, 164–174 (2009). doi:10.1111/j.1365-246X.2008.03966.x

39. F. Brenguier, P. Boué, Y. Ben-Zion, F. Vernon, C. W. Johnson, A. Mordret, O. Coutant, P.-E. Share, E. Beaucé, D. Hollis, T. Lecocq, Train Traffic as a Powerful Noise Source for Monitoring Active Faults With Seismic Interferometry. *Geophys. Res. Lett.* **46**, 9529–9536 (2019). doi:10.1029/2019GL083438 Medline

40. T. Lecocq *et al*., ThomasLecocq/2020_Science_GlobalQuieting: First Release - v1.0, Zenodo (2020); https://doi.org/10.5281/zenodo.3944739.

41. A. Aktay, S. Bavadekar, G. Cossoul, J. Davis, D. Desfontaines, A. Fabrikant, E. Gabrilovich, K. Gadepalli, B. Gipson, M. Guevara, C. Kamath, M. Kansal, A. Lange, C. Mandayam, A. Oplinger, C. Pluntke, T. Roessler, A. Schlosberg, T. Shekel, S. Vispute, M. Vu, G. Wellenius, B. Williams, R. J. Wilson, Google COVID-19 Community Mobility Reports: Anonymization Process Description (version 1.0). arXiv:2004.04145 [cs.CR] (8 April 2020).

42. M. Schäfer, M. Strohmeier, V. Lenders, I. Martinovic, M. Wilhelm, in *IPSN-14 Proceedings of the 13th International Symposium on Information Processing in Sensor Networks* (IEEE, 2014), pp. 83–94.

43. S. R. Proud, Go-Around Detection Using Crowd-Sourced ADS-B Position Data. *Aerospace* **7**, 16 (2020). doi:10.3390/aerospace7020016

44. D. E. McNamara, R. I. Boaz, "PQLX: A Seismic Data Quality Control System Description, Applications, and Users Manual" (Open-File Report 2010-1292, U.S. Geological Survey, 2010).

45. R. E. Anthony, A. T. Ringler, D. C. Wilson, M. Bahavar, K. D. Koper, How Processing Methodologies Can Distort and Bias Power Spectral Density Estimates of Seismic Background Noise. *Seismol. Res. Lett.* **91**, 1694–1706 (2020). doi:10.1785/0220190212

46. M. Beyreuther, R. Barsch, L. Krischer, T. Megies, Y. Behr, J. Wassermann, ObsPy: A Python Toolbox for Seismology. *Seismol. Res. Lett.* **81**, 530–533 (2010). doi:10.1785/gssrl.81.3.530

47. T. Megies, M. Beyreuther, R. Barsch, L. Krischer, J. Wassermann, ObsPy – What can it do for data centers and observatories? *Ann. Geophys.* **54**, 47–58 (2011). doi:10.4401/ag-4838

48. L. Krischer, T. Megies, R. Barsch, M. Beyreuther, T. Lecocq, C. Caudron, J. Wassermann, ObsPy: A bridge for seismology into the scientific Python ecosystem. *Comput. Sci. Discov.* **8**, 014003 (2015). doi:10.1088/1749-4699/8/1/014003

49. R. B. Blackman, J. W. Tukey, The measurement of power spectra from the point of view of communications engineering—Part I. *Bell Syst. Tech. J.* **37**, 185–282 (1958). doi:10.1002/j.1538-7305.1958.tb03874.x

50. P. Welch, The use of fast Fourier transform for the estimation of power spectra: A method based on time averaging over short, modified periodograms. *IEEE Trans. Audio Electroacoust.* **15**, 70–73 (1967). doi:10.1109/TAU.1967.1161901

51. J. D. Hunter, Matplotlib: A 2D Graphics Environment. *Comput. Sci. Eng.* **9**, 90–95 (2007). doi:10.1109/MCSE.2007.55

52. R. Lacassin, M. Devès, S. P. Hicks, J.-P. Ampuero, R. Bossu, L. Bruhat, D. F. Wibisono, L. Fallou, E. J. Fielding, A.-A. Gabriel, J. Gurney, J. Krippner, A. Lomax, M. M. Sudibyo, A. Pamumpuni, J. R. Patton, H. Robinson, M. Tingay, S. Valkaniotis, Rapid collaborative knowledge building via Twitter after significant geohazard events. *Geosci. Commun.* **3**, 129–146 (2020). doi:10.5194/gc-3-129-2020

53. T. Kluyver *et al*., in *Positioning and Power in Academic Publishing: Players, Agents and Agendas: Proceedings of the 20th International Conference on Electronic Publishing*, F. Loizides, B. Schmidt, Eds. (IOS Press, 2016), pp. 87–90.

54. T. Lecocq, F. Massin, C. Satriano, M. Vanstone, T. Megies, SeismoRMS - A simple Python/Jupyter Notebook package for studying seismic noise changes, Version 1.0, Zenodo (2020); http://doi.org/10.5281/zenodo.3820046.

55. L. Krischer, Y. A. Aiman, T. Bartholomaus, S. Donner, M. Driel, K. Duru, K. Garina, K. Gessele, T. Gunawan, S. Hable, C. Hadziioannou, M. Koymans, J. Leeman, F. Lindner, A. Ling, T. Megies, C. Nunn, A. Rijal, J. Salvermoser, S. T. Soza, C. Tape, T. Taufiqurrahman, D. Vargas, J. Wassermann, F. Wölfl, M. Williams, S. Wollherr, H. Igel, seismo-live: An Educational Online Library of Jupyter Notebooks for Seismology. *Seismol. Res. Lett.* **89**, 2413–2419 (2018). doi:10.1785/0220180167

56. QGIS Development Team, QGIS Geographic Information System, Open Source Geospatial Foundation (2020); https://qgis.org/en/site/.